International Journal of Engineering Research & Technology (IJERT)
ISSN: 2278-0181
Vol. 9 Issue 07, July-2020

Removal of Methyl Orange (MO) by Chitosan Modified by Zero Valent Iron

M.A. Conde[1], Careme. L. S. Liwaire[1], Armand N. Tchakounte[1],
Clandy .A. S. Ntinkam[1], Dave. L. E. Nzugue[1], Charles M. Kede[1,2]*.
[1]Department of Chemistry, Faculty of Science, University of Douala, P.O. Box 24175, Douala, Cameroon.
[2]Department of Process Engineering National Higher Polytechnic School of Douala, University of Douala, P.O. Box 2701, Douala, Cameroon.

***Abstract*— This work focuses on MO sorption by chitosan, nZVI/chitosan and nZVI was investigated. The purpose of this study is to understand the mechanisms that govern the elimination of MO and to find a suitable kinetics model of removal. Spectroscopic studies including FTIR, (TG-DSC), Methylene blue and Iodine number and effect of pH were used for its characterization. Equilibrium data was examined using a comparison of linear Langmuir, Freundlich and Temkin isotherm models. The Freundlich isotherm provided the best fit to the experimental data for MO as indicated by the values of the regression coefficient. The kinetic rates were modeled by using the Lagergren-first-order, pseudo-second-order, Elovich and Intraparticle diffusion model. The pseudo-second-order model was found to explain the adsorption kinetics most effectively. The presence of intra-particle diffusion mechanism was prominent, although it was not the sole rate-determining step. The results showed that Chitosan, nZVI/ Chitosan and nZVI, can be effective for removing MO from solution.**

Keywords*— Adsorption; Chitosan; Nanoparticle; zero valent iron; Methyl orange

1. INTRODUCTION

Water touches all aspects of development and it is the center of almost all of the goals of sustainable development. It stimulates economic growth, promotes healthy ecosystems and is essential for life. Faced with strong demographic growth, humanity has resorted to industrialization and modernization to meet its needs. Paradoxically, this industrialization causes damage to the environment. Particularly the massive production of solid waste, water pollution due to the dumping of a wide variety of chemicals (synthetic dyes, heavy metals and many others) in the water cycle thus endangering this resource.

Indeed, in printing houses, food industries, cosmetics and pharmaceuticals, but especially in the textile industry (Talarposhti and al., 2001), dyes are widely used for their chemical stability, ease of their synthesis and color variety. These dyes, in this case methyl orange, are at the origin of pollution once discharged into the environment. Studies have shown that several azo dyes are toxic and mutagenic (Hedi and al., 2011). The heterogeneity of their composition makes it difficult if not almost impossible to obtain pollution thresholds lower or equal to those imposed by environmental standards, after treatment with traditional techniques. Several conventional techniques have been developed to remove dyes from water, the best known and most used are the biological and physico-chemical methods (coagulation/flocculation, reverse osmosis, chemical oxidation, ion exchange, electrochemical methods). In addition, energy demand is high (Rangabhashiyam and al., 2013). For several decades, adsorption has not ceased to seduce the scientific community because in general, it is a simple separation process, inexpensive, free of byproducts and above all effective. The speed, reversibility, and simplicity of the apparatus constitute the main advantages of adsorption as a technique for removing organic and inorganic pollutants in water. Adsorbents commonly used are activated carbon, polymeric materials, clays, biosorbents (Rajkumar and al., 2014). Research work has been conducted to develop adsorbent materials at low cost using natural waste from agriculture and animals. The use of this waste for the synthesis of adsorbent materials contributes to the protection of the environment, the reduction of waste disposal costs and the valorization of these. We were interested in the synthesis of an available and inexpensive adsorbent, chitosan prepared from the crab shells for the elimination of methyl orange. These shells come from the recycling of discharges from the fishing industry, animal waste available throughout Cameroon. Some adsorbents are characterized by a low adsorption capacity, higher cost, a longer equilibrium time, and low regeneration capacities. To improve their performances, one can proceed by incorporating additional chemical substances capable of giving them magnetic properties. This method has been widely used in recent years due to its simplicity and high speed.

Habiba and collaborators obtained a maximum adsorption capacity of 416.1 mgg^{-1} for the absorption of methyl orange on a nano-composite of chitosan glyoxal (Habiba and al., 2018). Mohammad et al, synthesized a composite nano fibrous chitosan-alcohol-polyvinyl-zeolite membrane for the adsorption of methyl orange. The adsorption capacity of the membrane was 153 mgg^{-1} (Mohammad et al., 2019). In 2010 Zhang et al, showed that more than 98% of Pb^{2+} ions in wastewater had been eliminated using kaolinite impregnated with zero iron nanoparticles. A similar approach gives us the enthusiasm to study carefully the elimination of a dye: methyl orange by a biosorbent impregnated with zero iron.

So far, the removal of MO using (CHT, CHT/nZVI, nZVI) adsorbent has not been a lot reported in the literature. Hence, the main objective of this investigation was to examine adsorption characteristic for MO on modified CHT by iron nanoparticles (CHT/nZVI) coated on it. The effects of such

International Journal of Engineering Research & Technology (IJERT)
ISSN: 2278-0181
Vol. 9 Issue 07, July-2020

factors as contact time, pH, as well as isotherm and adsorption kinetics were also studied.

2. MATERIALS AND METHODS

2.1. Sampling area and adsorbent.

The crab shells used as raw material in this study comes from the mangrove of Youpwe, Douala Cameroon (4°8'N and 9°49'E). Then the sample was grinded in a mortar and sieved as to pass through 125 μm mesh size. The Biomaterial sample was stored in sterile, closed plastic containers and used as an adsorbent.

2.2. Preparation of CHT

Production of this chitosan is based on chitin derived from shells of crabs. The steps in the extraction of chitin from shells are the removal of proteins and minerals, such as calcium carbonate and calcium phosphate, by treatment with alkali and acid respectively. Before chemical treatment, the shells are grind to improve the efficiency of treatment, and after final rinsing the chitin are dried and can be stored as a stable intermediate. The deacetylation of chitin through treatment with strong NaOH is carried out at elevated temperature over a controlled period of time. To achieve the highest possible yield the material is kept in the solid state. To prepare a filterable grade product, an additional step is added, including solubilization in an appropriate organic acid. The acid solution is then filtered through specified mesh size filter before spray drying. In contrast to the regular grade chitosan, this latter form is water soluble. Water-soluble industrial-grade chitosan is made by regular dry blending of chitosan with an appropriate acid. These chitosan production processes are summarized in Fig.1.

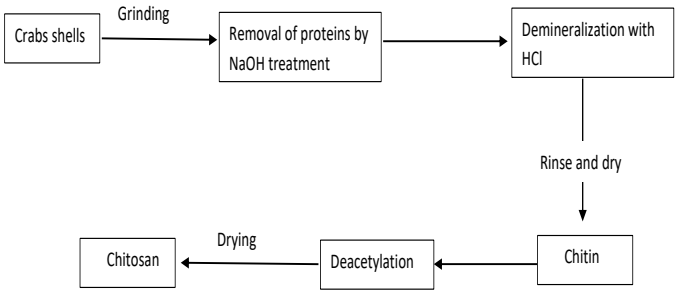

Fig1. Scheme of the procedure of Chitosan preparation

2.3. Preparation of nZVI and CHT/nZVI

Green tea extract was prepared by heating 20 g/L green tea to 80 °C followed by vacuum filtration. A solution of 0.1M $Fe_2SO_4.7H_2O$ was prepared by dissolving 16.2 g of solid $Fe_2SO_4.7H_2O$ in 1 L of deionized water. Green tea synthesized nanoscale zero-valent iron (nZVI) was then prepared by adding 0.1M $Fe_2SO_4.7H_2O$ to 20 g/L green tea in a 2:1 volume ratio (Hoag and al 2009).

To obtain CHT/nZVI, 10g of chitosan was added to a solution of 0.1 M $Fe_2SO_4.7H_2O$ then stirred for 45 minutes. To obtained mixture a solution of 20g/L of green tea was added. The CHT/nZVI were separated and immediately washed many times with water and dried.

2.4. Adsorbate preparation

All the chemicals used in the present work were of analytical reagent grade obtained from Aldrich Chemical Co. A methyl orange stock solution of 1000 mgL^{-1} was prepared by mixing 1 g of methyl orange in 1 L of de-ionized water. This stock solution was serially diluted to get the appropriate concentrations for conducting adsorption experiments.

2.5. Solid-Phase Characterization of CHT, CHT/nZVI and nZVI

The pH at the potential of zero charge of the CHT, CHT/nZVI and nZVI was measured using the pH drift method. The pH of the solution was adjusted by using 0.01 M sodium hydroxide or hydrochloric acid. Nitrogen was bubbled through the solution at 250 °C to remove the dissolved carbon dioxide 100 mg was added to 50 ml of the solution. After stabilization, the final pH was recorded. The graphs of final pH versus initial pH used to determine the zero-point charge of the CHT, CHT/nZVI and nZVI (lopez and al, 1999).

The CHT, CHT/nZVI and nZVI, activation temperature was fixed using thermogravimetry and differential thermal analysis (TG- DSC). A Fourier transform infrared spectroscope (FTIR, Nicolet 6700, Nicolet, USA) was used to evaluate the distribution of functional groups on the surface between different materials at a resolution of 2 cm^{-1}.

2.6. Aqueous Adsorption Characteristics

2.6.1. Iodine number

The iodine number was determined by using the sodium thiosulfate volumetric method. Standard iodine solution was added over adsorbents (100 mg) and after an equilibration time of 5 min, the residual iodine concentration was determined by titration with standard sodium thiosulfate using starch as an indicator. The iodine number was defined as the adsorbed quantities of iodine ($mol.g^{-1}$ of adsorbents) obtained by subtracting the residual concentration at equilibrium C_e, from the initial concentration C_0

$$Q_0 = \frac{C_0 - C_e}{m} V \quad (1)$$

Where m and V are the mass of adsorbents sample and the volume of adsorbing solution respectively.

2.6.2. Methylene blue adsorption test

The samples of CHT, CHT/nZVI and nZVI were investigated for their aqueous adsorption of dyes using methylene blue. adsorbents samples (100 mg) were mixed with methylene blue in 50 mL stoppered erlenmeyer flasks. Batch experiments were carried out in the shaker at room temperature for 2h. The solutions were filtered and the concentrations of solutions were then determined by spectrophotometer at 659 nm. Then the quantity adsorbed was also calculated ($mol.g^{-1}$) for CHT, CHT/nZVI and nZVI using equation (1).

International Journal of Engineering Research & Technology (IJERT)
ISSN: 2278-0181
Vol. 9 Issue 07, July-2020

2.7. Batch adsorption studies

The adsorbate stock solution of 1000 mgL^{-1} of methyl orange was diluted as required to obtain standard solutions containing 10 to 60 mgL^{-1}. Batch mode adsorption studies were carried out with 50 mg of adsorbent and 50 mL of methyl orange solution of a desired concentration in 200 mL conical flasks and were agitated for predetermined time intervals at room temperature in a mechanical shaker. The removal kinetics of methyl orange were investigated by taking samples of the solution after the desired contact time (0–120 min). The residual concentration of methylene blue was determined using Spectroquant Pharo 300 spectrophotometer at 465 nm.

3. RESULTS AND DISCUSSIONS

3.1. Characterization of CHT, CHT/nZVI and nZVI

This spectra range from 4,000 to 500 cm^{-1}. The broad bands at 3292 cm^{-1}, 3254 $cm^{-1}$and 3209 cm^{-1} for CHT, CHT/nZVI and nZVI respectively are attributed to intermolecular hydrogen bonds and to the elongation vibration overlap between the O-H and N-H bonds. In addition, the 2876 cm^{-1} band for CHT corresponds to the elongation vibrations of the aliphatic C-H bonds (Du and al., 2014). The peaks at 1654 cm^{-1} ,1620 cm^{-1} and 1614 cm^{-1} respectively for CHT, CHT/nZVI and nZVI correspond to the elongation vibration of the C=O bond of the carbonyl group. The peaks at 1419 cm-1 and 1375 cm-1 for CHT, 1425 cm^{-1}, 1375 cm^{-1} for CHT/nZVI and 1423 and 1338 cm^{-1} for nZVI correspond to the C-N bond (Malkoc and al., 2014). The peaks at 1149 cm^{-1} for CHT, 1151 cm^{-1} for CHT/nZVI and 1202 cm^{-1} for nZVI are those of the C-O-C bond. The vibration of the C-O bond of alcohols is characterized by bands at 1058 cm^{-1} for CHT, 1072 cm-1 for CHT/nZVI and 1075 cm^{-1} for nZVI (Reddy and al., 2007). The bands 1026 cm^{-1} for CHT, 1008 cm^{-1} for CHT/nZVI and 1017 cm^{-1} for nZVI are characteristic of the O-C bond. However, out-of-plane vibration of the C-H link is characterized by peaks at 892 cm-1 for CHT, 952 cm^{-1} for CHT/nZVI. On the other hand, peaks at 514 and 440 CHT/nZVI, 592 and 512 for nZVI are characteristic of the Fe-O bond (Yang et al., 2014). We note that the characteristic peaks of the C-H and C-O-C bonds of the CHT have almost disappeared in the CHT/nZVI, the characteristic peaks of the C=O, N-H and C-N bonds of the CHT are more intense in the CHT/nZVI, the characteristic peaks of the Fe-O bond are present on the CHT/nZVI, nZVI and absent on the CHT. The impregnation with nZVI has therefore changed the structure of the CHT/nZVI by opening the heterocycles, removing the methyl groups and incorporating the iron into the matrix of the latter.

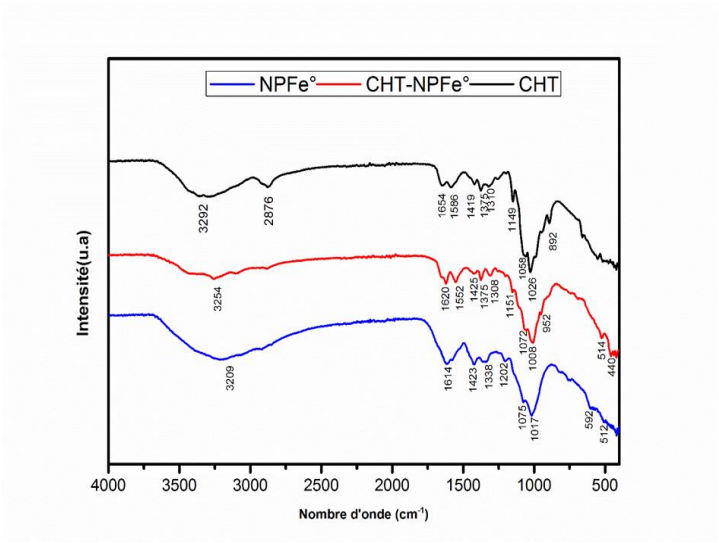

Fig2. FTIR spectra of CHT, CHT/nZVI and nZVI

The result of thermogravimetric analysis of CHT, CHT/nZVI and nZVI coupled with differential scanning calorimetry are shown in the fig 3, 4 and 5.

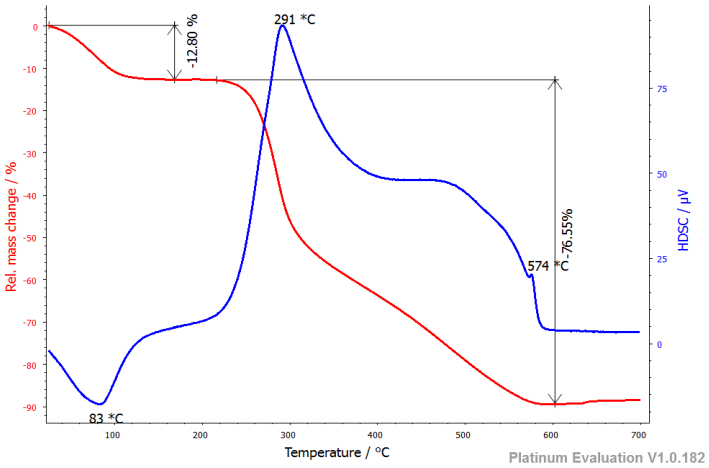

Fig 3. Curve of thermo-gravimetric analysis (TG and DSC) of CHT

From Fig.3 which represents the thermogram of CHT, we note that the thermal degradation profile occurs in two stages. The first indicates the loss of water in the sample and appears in the area between 50 ° C to 110 ° C and correspond to a loss of mass of 12.80%. The second loss of mass (with a high speed of loss of mass) is recorded in the temperature range between 250 ° C - 410 ° C corresponding to a mass loss of 76.55% can be attributed to the degradation of the polymer chain of chitosan. Mass loss continues gradually and slowly up to 600 ° C.

International Journal of Engineering Research & Technology (IJERT)
ISSN: 2278-0181
Vol. 9 Issue 07, July-2020

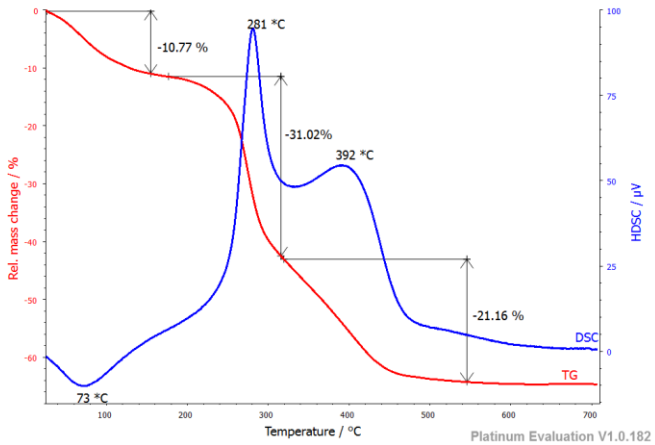

Fig 4. Curve of thermo-gravimetric analysis (TG and DTG) of CHT/nZVI

The thermal decomposition of CHT/nZVI (fig.4) occurs in three steps. The first and the second steps correspond to the evaporation of water and the degradation of the polymer chain of chitosan respectively, while the third step corresponds to a weigth loss of 21.16% in the temperature range of 350 °C to 650 °C. This loss of mass is attributed to the degradation of the organic matter resulting from the impregnation of the chitosan by the nanoparticles of iron zero.

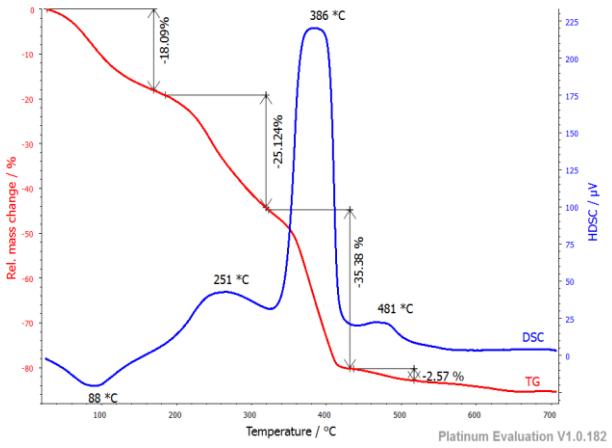

Fig 5. Curve of thermo-gravimetric analysis (TG and DTG) of nZVI

Iodine and methylene blue adsorption are considered as simple and quick test for evaluating

the porous structure of micro and mesoporous adsorbents. Iodine has a small molecular size and can readily penetrate deep micropores of the CHT, CHT/nZVI and nZVI. So iodine number gives approximate measure of the micropore content of the CHT, CHT/nZVI and nZVI. Likewise, methylene blue number indicates the mesopore distribution in the adsorbents and indicates the ability of CHT, CHT/nZVI and nZVI to adsorb medium size molecules. IN and MBN of CHT, CHT/nZVI and nZVI is shown in (Fig.5 and table 1) CHT, CHT/nZVI and nZVI are essentially micropores with a more pronounced microporosity for nZVI.

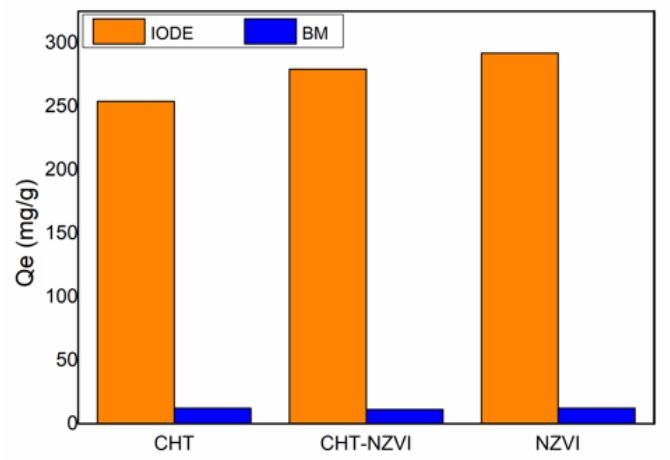

Fig.6. Adsorption of iodine and methylene blue *onto* CHT, CHT/nZVI and nZVI

Table 1: Physicochemical properties of CHT, CHT/nZVI and nZVI

Biosorbent	Methylene blue number (mg/g)	$S_{MB}(m^2 g^{-1})$	Iodine number (mg/g)	$S_{IN}(m^2 g^{-1})$	p_{ZPC}^{H}
CHT	12.172	29.799	257	325.120	7.8
CHT/nZVI	11.110	24.452	279.4	357.632	5.0
nZVI	12.237	29.956	292.1	373.888	4.0

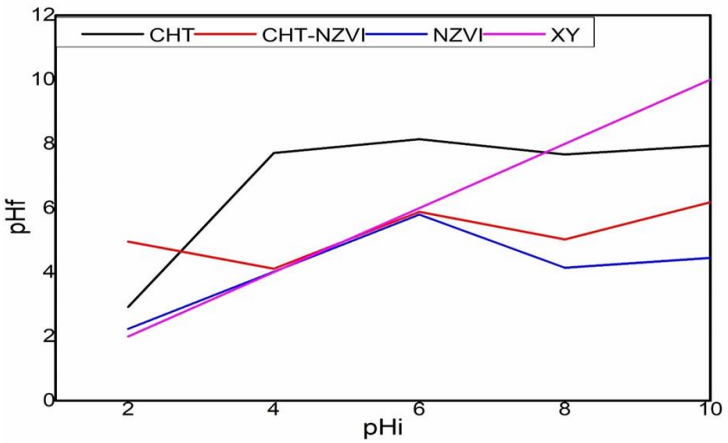

Fig.7. pH zero-point charge of CHT, CHT/nZVI and nZVI

The value of pH_{ZPC} is 7.8 for CHT, it is therefore of a basic nature and on its surface, basic groups are predominant. However, the pH_{ZPC} values of CHT/nZVI and nZVI are 5 and 4 respectively, they are acidic in nature and acidic groups are predominant on their surfaces. These values tell us the suitable range for the adsorption of methyl orange. When the pH is lower than the pH_{ZPC} the surface of CHT/nZVI is protonated, it is positively charged. At pHs above pH_{ZPC} the hydroxyl ions neutralize the positive sites and the surface then charges negatively. In addition, at pH below the P_{Ka} of methyl orange (3.9) it occurs in the cationic form (acid) and develops a repulsion opposite the adsorbent.

3.2. Effect of contact time

The time necessary to reach the equilibrium of adsorption of MO onto CHT, CHT/nZVI and nZVI was investigated at

International Journal of Engineering Research & Technology (IJERT)
ISSN: 2278-0181
Vol. 9 Issue 07, July-2020

initial concentration of 50 mg/l. Experiments were performed using a solid-liquid ratio of 1 g/l and lack of the other number. The variation of adsorption capacity as function of contact time for MO on CHT, CHT/nZVI and nZVI, are shown in Fig.8. Results indicate that the rate of adsorption of MO are fast for the first 5 min and thereafter slowed gradually until the adsorption reaches equilibrium at about 45 min. A large number of vacant active sites are occupied by the MO during the initial time of contact. After a period of time, the vacant surface sites are difficult to be available because of the repulsive forces between the MO adsorbed on CHT, CHT/nZVI and nZVI surface and the MO in solution. Therefore, the mesopores on the surface of CHT, CHT/nZVI and nZVI were saturated with MO in the initial stage of adsorption. Thereafter, the MO have to traverse farther and deeper into the pores encountering much larger resistance (L. Khalfa et al, 2016).

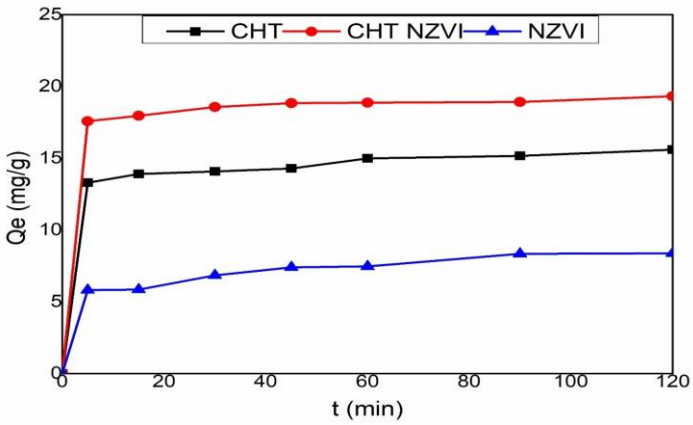

Fig.7. *Kinetic curves of contact time on* MO *adsorption onto* CHT, CHT/nZVI and nZVI.

3.3 Effect of pH

Fig 8 shows the effect of the initial pH on the adsorption of methyl orange by CHT, CHT/nZVI and nZVI for a dye concentration of 20 mg/L. The adsorption capacity is maximum in an acid medium, more precisely when the pH value is lower than the pH_{ZPC} of each of the adsorbents. A general observation of the figure shows that the amount of orange methyl adsorbed decreases when the pH value is higher than pH_{ZPC}. This phenomenon is justified by the acid-base behavior of methyl orange. Indeed, the orange methyl is an anionic dye (carries the negative charge), in acid medium the H^+ ions are predominant in the solution; therefore, the vacant sites of the adsorbent will be occupied by these cations, and the orange methyl molecules will be adsorbed by the positive sites of the support. In other words, as the pH of the system increases, the number of negatively charged sites increases unlike that of the positively charged sites which decreases. The negative charge of the adsorbent sites therefore does not promote the adsorption of the dye anions due to electrostatic repulsion. In addition, the low adsorption rate of methyl orange at alkaline pH is due to the presence of excess OH- ions, which will compete with the anionic molecules of dye for the adsorption sites.

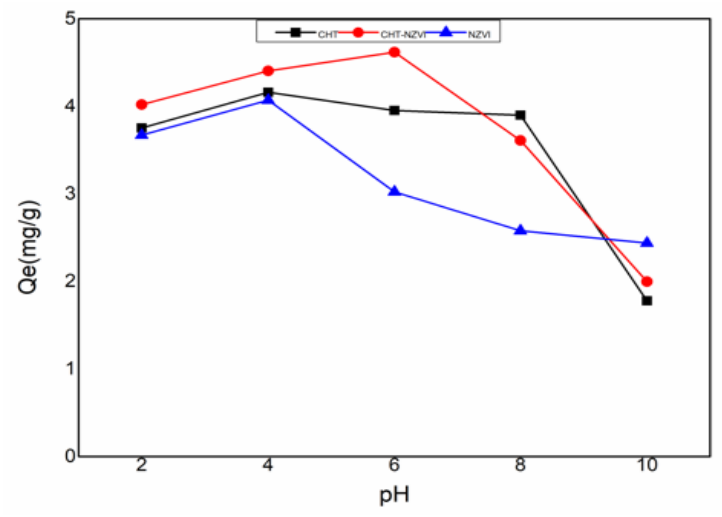

Fig 8: influence of pH variation on biosorbents adsorption capacity

3.4 Kinetic Studies

The adsorption kinetic study is important for determining the efficiency of adsorption and for determination of the adsorption rate limiting steps being necessary in order to define the rate parameters for design purposes. Kinetic data obtained from the adsorption study of MO were predicted with different models widely applied to describe the adsorption behavior of MO on CHT, CHT/nZVI and nZVI. In order to determine the mechanism of adsorption and its potential rate controlling step, the tested models were: The pseudo-first order model (Nekouei and al, 2015) pseudo-second order model and intraparticle diffusion model (Belaid and al, 2013).

Pseudo-first-order:

$$\log(q_e - q_t) = \log q_e - \frac{k_1 t}{2.303} \quad (2)$$

Pseudo-second-order:

$$\left(\frac{t}{q_t}\right) = \left(\frac{t}{q_e}\right) + \left[\left(\frac{1}{k_2 q_e^2}\right)\right] \quad (3)$$

Intraparticle diffusion model:

$$q = f\left(\frac{D_t}{r_p^2}\right)^{1/2} = k_w t^{1/2} + C \quad (4)$$

where q_e (mg/g) is the equilibrium adsorption amount, q_t (mg/g) is the adsorption amount at time t(min), $k_1(min^{-1})$, $k_2(g/mg.min^{-1})$ are constant of the pseudo-first-order, the pseudo-second-order, respectively, and $k_p(mg/g.min^{1/2})$ intraparticle diffusion constant rates, C is proportional to the boundary layer thickness.

The pseudo-first-order and pseudo-second order kinetic models were applied to predict the mechanism involved in the adsorption process of MO. The linear form of the pseudo and second order model were given by (2) and (3). It is clear from

International Journal of Engineering Research & Technology (IJERT)
ISSN: 2278-0181
Vol. 9 Issue 07, July-2020

obtained data of Table 2 that pseudo second order kinetic model is more able to provide a successful description of MO adsorption onto CHT, CHT/nZVI and nZVI. The kinetic parameters and the correlation coefficients values determined from the slope and the intercept of these plots are illustrated in Table 2. The calculated adsorptive capacities values from the pseudo- second order model are in a good agreement with those experimentally determined. Moreover, the correlation coefficient values are quite well > 0,982, and much higher than those found by the pseudo-first order kinetic model. Thus, we can assert that the adsorbent systems are well described by the pseudo-second order kinetic model.

Intraparticle diffusion model is given by (4). It can be seen from curves regarding the effect of contact time, three distinct steps: the external diffusion, the intraparticle diffusion and equilibrium stage. The first slopes covering the time range between 0-5 min, must be the external diffusion. This is related to the binding of MO by active sites which are distributed onto the outer surface of the adsorbents. The second linear portions included the adsorption period of 5-45 min, is assigned to the gradual adsorption limited by diffusion of MO in the micropores of the adsorbent particles: the intraparticle diffusion. The third linear portions included the time period of 45-120 min, which denotes establishment of the equilibrium. The values of the correlation and the diffusion rate constants were determined from the Weber and Morris model and reported in Table 2. High correlation coefficient values suggest an important relationship between qt and $t^{1/2}$ resulting from the adsorption of MO onto CHT, CHT/nZVI and nZVI.

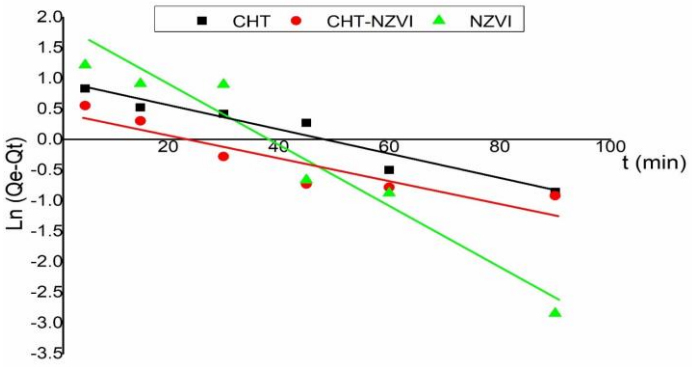

Fig.9. Pseudo-first order kinetic plots for MO adsorption onto CHT, CHT/nZVI and nZVI.

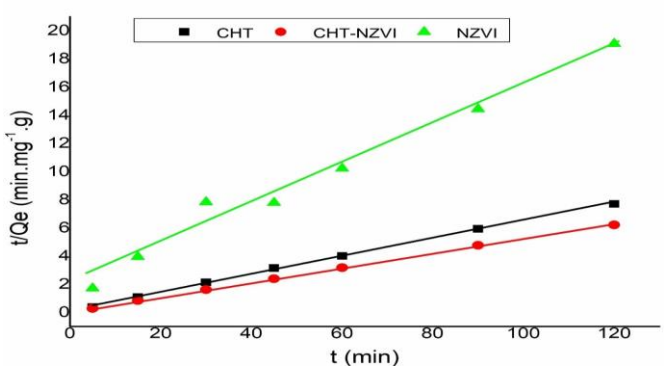

Fig.10. Pseudo-second order kinetic plots for MO adsorption onto CHT, CHT/nZVI and nZVI

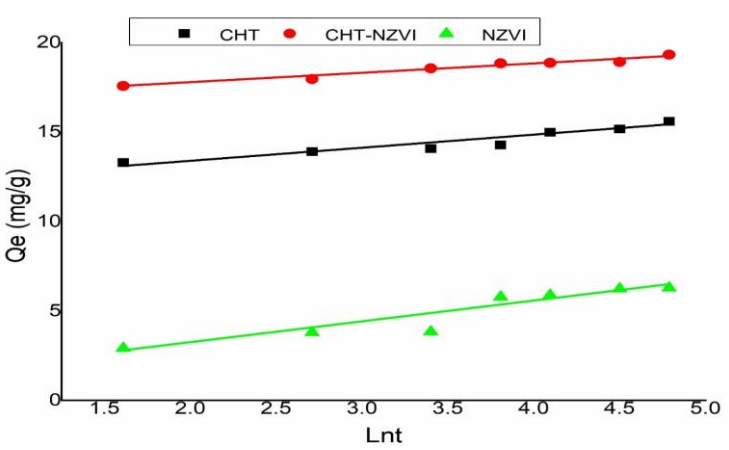

Fig. 11. Elovich kinetic plots for MO adsorption onto CHT, CHT/nZVI and nZVI.

Table 2: Kinetics parameters for MO adsorption onto CHT, CHT/nZVI and nZVI

Adsorbents	Lagergren		Pseudo second-order				Intraparticular diffusion		
	K_1/min^{-1}	R^2	K_2/g.mg^{-1}min^{-1}	h/g.mg^{-1}min^{-1}	Q_e(mg/g)	R^2	K_d/ mg.g.min$^{-1/2}$	I	R^2
CHT	0,020	0,938	0,024	5,902	15,748	0,999	0,259	1,275	0,966
CHT/nZVI	0,018	0,837	0,045	16,911	19,342	0,999	0,189	1,732	0,914
nZVI	0.048	0.946	0,011	0,548	8,293	0,982	0.426	2,132	0,872

3.5 Equilibrium isotherms

The isotherm adsorption studies were investigated to determine the maximum adsorption uptake for MO on CHT, CHT/nZVI and nZVI. Isotherms were evaluated using the commonly used equilibrium model: Langmuir, Freundlich and Temkin models (Tchakounte and al; 2019).

Langmuir linear equation:

$$\frac{C_e}{Q_e} = \frac{1}{K_L Q_{\max}} + \frac{1}{Q_{\max}} C_e \qquad (5)$$

where Q_e is the equilibrium MO concentration on the adsorbent (mgg^{-1}), Ce is the equilibrium (MO) concentration in the solution (mgL^{-1}), Q_{max} adsorbent (mgg^{-1}), and K_L is the monolayer adsorption capacity of the Langmuir adsorption constant (Lmg^{-1}) related with the free energy of adsorption. (Fig. 9 and table 3) indicate the linear relationship between the amount (mg) of MO sorbed per unit mass (g) of CHT, CHT/nZVI and nZVI against the concentration of MO remaining in solution (mg/L). The coefficients of correlation(R^2) grouped in table 3 indicate that the adsorption of the MO onto CHT, CHT/nZVI and nZVI don't fit well the Langmuir model. In other hands, the sorption of MO onto CHT, CHT/nZVI and nZVI was taken place at the functional groups/binding sites on the surface of the CHT, CHT/nZVI and nZVI which is regarded as monolayer biosorption.

International Journal of Engineering Research & Technology (IJERT)
ISSN: 2278-0181
Vol. 9 Issue 07, July-2020

Table 3. Freundlich, Langmuir and Temkin isotherms constants for methylene blue adsorption onto CHT, CHT/nZVI and nZVI.

	Freundlich			Langmuir			Temkin		
Adsorbents	K_f	N	R^2	K_L	R_L	R^2	B_T	A_T	R^2
CHT	0.994	2.795	0.911	0.018	0.358	0.234	0.175	0.877	0.836
CHT/nZVI	1.429	1.355	0.912	0.031	0.347	0.679	0.155	2.713	0.904
nZVI	0.944	1.537	0.984	0.029	0.486	0.709	0.270	1.319	0.594

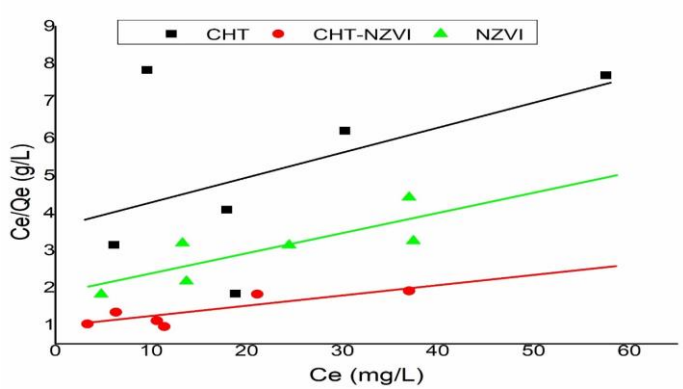

Fig.12. Langmuir adsorption isotherm for removal of MO onto CHT, CHT/nZVI and nZVI

The Freundlich model assumes active sites of differents energies and a heterogeneous adsorption surface.
The Freundlich model (Kede et al.2015) is

$$\log\left(\frac{x}{m}\right) = \log K_F + \frac{1}{n}\log C_e \qquad (6)$$

Where K_F is a constant relating the adsorption capacity and 1/n is an empirical parameter relating the adsorption intensity, which varies with the heterogeneity of the material (Fig.10 and table 3). The higher R^2 of the Freundlich model implied a greater tendency of the heterogeneous surface of CHT, CHT/nZVI and nZVI for the removal of MO. The low value of 1/n in the Freundlich isotherm suggested that any large change in the equilibrium concentration of MO would not result in a significant change in the amount of MO adsorbed by CHT, CHT/nZVI and nZVI. The Freundlich constant n is found to be greater than 1 which indicates a favourable condition for adsorption (Rongbing and al, 2015).

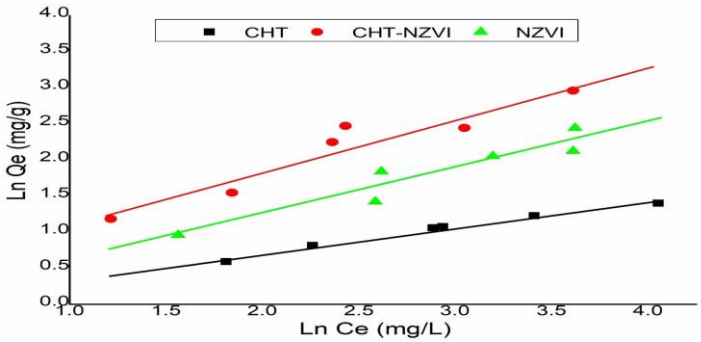

Fig.13. Freundlich adsorption isotherm for removal of MO onto CHT, CHT/nZVI and nZVI

The Temkin isotherm contains a factor that explicitly takes into account of the adsorbent-adsorbate interactions. In this equation, it is assumed that, because of these interactions and ignoring very low and very large concentration values, the heat of adsorption of all molecules in the layer would decrease linearly with the coverage (Lalhruaitluanga and al.2010). The linear form of the Temkin model is written as:

$$Qe = B\ln A_T + B\ln Ce \qquad (7)$$

where A_T is the equilibrium binding constant corresponding to the maximum binding energy, $B=RT/b_T$, b(J/mol) is the Temkin constant related to the heat of adsorption, R (8.314 J/mol K) is the universal gas constant and T (K) is solution temperature.
The values obtained from the Temkin isotherm (Fig.11 and table 3), indicate that the adsorption of (MO) onto CHT, CHT/nZVI and nZVI occurred via chemisorption. The values for A_T were higher than 8 kJ mol^{-1} and thus the mechanism involved is chemical adsorption. In the chemisorption process, the adsorbates adhere to the adsorbent through a weak chemical bond and thus this process is associated with relatively higher adsorption energies (Hardiljeet and al.2011).

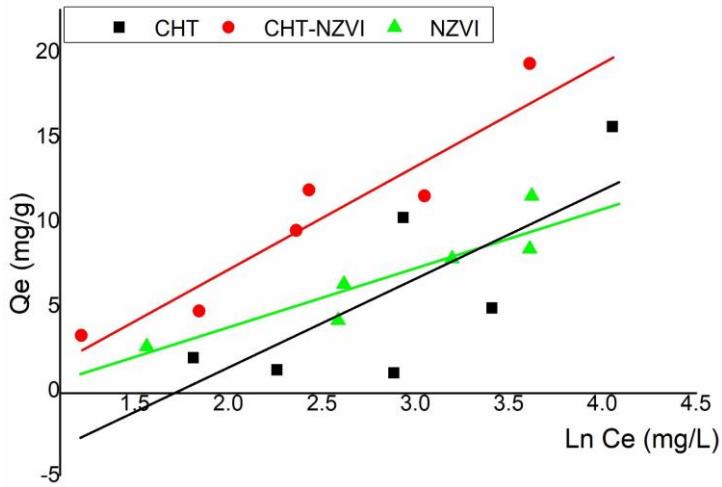

Fig.14. Temkin adsorption isotherm for removal of MO onto CHT, CHT/nZVI and nZVI.

4. CONCLUSIONS

In this work, the removal of Methyl orange from aqueous solution onto CHT, CHT/nZVI and nZVI has been investigated. The adsorption results showed that the CHT/nZVI is an effective adsorbent for removal MO with high adsorption uptake (19.31 mg/g) under the optimum operating condition: 120 min contact time and adsorbent dose 1g/l. The Freundlich isotherm showed a better fit than the Langmuir and Temkin isotherms, thus, indicating the applicability of heterogeneity of (MO) on CHT, CHT/nZVI and nZVI. The adsorption kinetics was found to follow closely the pseudo-second-order kinetic model. Results from this study suggest that CHT, CHT/nZVI and nZVI are a very effective adsorbent for (MO).

Conflicts of interest

The authors declare no conflicts of interests.

International Journal of Engineering Research & Technology (IJERT)
ISSN: 2278-0181
Vol. 9 Issue 07, July-2020

REFERENCES

[1] Talarposhti AM, Donelly T, Anderson GK. (2001) Colour removal from a simulated dye wastewater using a two-phase anaerobic packed bed reactor, Water Res 35, 425–432

[2] Hedi, B., oualid, B., dorra D., barilliera, D., chekir-ghedirab, L., mosrati, R., (2011) les colorants textiles sources de contamination de l'eau : criblage de la toxicité et des méthodes de traitement Revue des sciences de l'eau. *Journal of Water Science*, vol. 24, 209-238.

[3] Rangabhashiyam, S., Anu, N., Selvaraju. N. (2013) Sequestration of dye from textile industry wastewater using agricultural waste products as adsorbents. *J of Envir Chem Engin*. 1, 629-641.

[4] Rajkumar, P., Kumar, P. S., Priyadharshini, M., Kirupha, S. D., Baskaralingam, P., & Sivanesan, S. (2014) Removal of Cu (II) ions from aqueous solution by adsorption onto activated carbon produced from Guazumaulmifolia seeds. *Environmental Engineering and Management Journal, 13, 905–914.*

[5] Habiba, Umma., Siddique, Tawsif A., Lee, Jacky Jia Li., Joo, Tan Chin., Ang, Bee Chin., & Afifi, Amalina M. (2018) Adsorption study of Methyl orange by Chitosan/Polyvinyl Alcohol/Zeolite Electrospun Composite Nanofibrous Membrane. Carbohydrate Polymers. *Carbohydrate Polymers Technologies and Applications*, 191, 79-85

[6] Mohammad, A.-T., Abdulhameed A.S., and Jawad, A.H., (2019) Box Behnken design to optimize the synthesis of new crosslinked chitosan-glyoxal/TiO_2 nanocomposite: Methyl orange adsorption and mechanism studies, *International Journal of Biological Macromolecules, 129, 98-109.*

[7] Zhang, X., Lin, S., Lu, X.Q., Chen, Z.L., (2010) Removal of Pb(II) from water using natural kaolin loaded with synthesized nanoscale zero-valent iron. *Chem. Eng. J.* 163, 243-248.

[8] Edvar Ons0yen & 0yvind Skaugrud., (1990) Metal recovery using chitosan. J. Chem. Tech. Biotechno, 49, 395-404

[9] George E. Hoag, John B. Collins, Jennifer L. Holcom Jessica R. Hoag, Mallikarjuna N. Nadagoud and Rajender S. Varma., (2009) Degradation of bromothymol blue by 'greener' nano-scale zero-valent iron synthesized using tea polyphenols. *J. Mater. Chem.*, 19, 8671–8677

[10] Lopez-Ramon M.V, Stoeckli. F, Morenco-Castilla. C, Carrasco-Martin F. (1999) On the caracrerization of acidic and basic surface site on carbons by various techniques. *Carbon*, 37, 215-1221.

[11] Du, Y., Pei, M., He, Y., Yu, F., Guo, W. & Wang, L. (2014) Preparation, characterization and application of magnetic Fe_3O_4-CS for the adsorption of orange I from aqueous solutions,. *PLoS one 9 (10), e108647*

[12] Malkoc, E. & Nuhoglu, Y. (2006) Fixed bed studies for the sorption of chromium (VI) onto tea factory waste. *Chemical Engineering Science, 61, 4363–4372.*

[13] Reddy, D. H. K. & Lee, S.-M. (2007) Application of magnetic chitosan composites for the removal of toxic metal and dyes from aqueous solutions. *Advances in Colloid and Interface Science 201, 68–93.*

[14] Yang, G., Tang, L., Lei, X., Zeng, G., Cai, Y., Wei, X., Zhou, Y., Li, S., Fang, Y. & Zhang, Y. (2014) Cd(II) removal from aqueous solution by adsorption on α-ketoglutaric acid-modified magnetic chitosan. *Applied Surface Science, 292, 710–716.*

[15] Leila Khalfa, M Luisa Cervera, Mohamed Bagane, Souad Souissi-Naja. (2016) Modeling of equilibrium isotherms and kinetic studies of Cr (VI) adsorption into natural and acid-activated clays. *Arabian Journal of Geosciences 9 (1), 75*

[16] Farzin Nekouei, Shahram Nekouei, Inderjeet Tyagi, Vinod Kumar Gupta. (2015) Kinetic, thermodynamic and isotherm studies for acid blue 129 removal from liquids using copper oxide nanoparticle-modified activated carbon as novel adsorbent. *Journal of Molecular Liquids 201, 124-133.*

[17] F. Al-Tohami, M. A. Ackacha , R. A. Belaid and M. Hamaadi. (2013) Adsorption of Zn (II) Ions from Aqueous Solutions by Novel Adsorbent: *Ngella sativa* Seeds. *APCBEE Procedia 5 400 – 404.*

[18] Armand N. Tchakounte, Harlette Z. Poumve, Charles M. Kede, J.M. Dika. (2019) Calcareous-support nanoscale Zero-valent iron: New findings on adsorption of Cr(VI) in aqueous solution. *Journal of Applied Surfaces and Interfaces, 6(1-3), 9-17*

[19] C.M.Kede, P.P. Ndibewu, M. Makonga. Kalumba, A. Nikolay. Panichev, H.M. Ngomo and J.M. Ketcha. (2015) Adsorption of Mercury (II) onto Activated Carbons derived from Theobroma cacao Pod Husk. *S. Afr.j. chem*. 68, 226-235.

[20] Rongbing Fu, Yingpin Yang, Zhen Xu, Xian Zhang, Xiaopin Guo, Dongsu Bi. (2015) The removal of chromium (VI) and lead (II) from groundwater using sepiolite-supported nanoscale zero-valent iron (S-NZVI). *Chemosphere 138, 726–734.*

[21] H Lahlruaitluanga, K Jayaram, M N V Prassad, K K Kumar. (2009) Lead (II) Adsorption from Aqueous Solutions by Raw and Activated Charcoals of Melocanna Baccifera Roxburgh (Bamboo)--A Comparative Study. *Journal of Hazardous Materials, 175(1-3), 311-8.*

[22] Hardiljeet K Boparia, Meera Joseph, Denis M O'Carroll. (2011) Kinetics and thermodynamics of cadmium ion removal by adsorption onto nano zerovalent iron particles. *Journal of hazardous materials, 186(1), 458-465.*